High-Resolution Solid-State ^{13}C and ^{15}N NMR Spectroscopy of Pyrazole and 3,5-Dimethylpyrazole Adsorbed on Alumina and Silica

Francisco Aguilar-Parrilla,[1a] Rosa M. Claramunt,[1b] Concepción López,[1b] Dionisia Sanz,[1b] Hans-Heinrich Limbach,*[,1a] and José Elguero*[1c]

Departamento de Química Orgánica y Biología, Facultad de Ciencias, UNED, Ciudad Universitaria, E-28040 Madrid, Spain; Instituto de Química Médica, C.S.I.C., Juan de la Cierva 3, E-28006 Madrid; and Institut für Organische Chemie der Freien Universität Berlin, Takustrasse 3, D-14195 Berlin, F.R.G.

Received: February 11, 1994®

High-resolution solid state ^{13}C and ^{15}N CPMAS NMR experiments (CP ≡ cross polarization, MAS ≡ magic angle spinning) have been performed on mixtures of pyrazole (**1**) and of 3,5-dimethylpyrazole (**2**) with alumina and silica, prepared both by mixing and mechanical grinding of the components and by solvent-assisted adsorption. A comparison of the spectra obtained with those of the bulk solids shows a strong dependence of the NH···N proton tautomerism on the environment. Whereas prototropy is suppressed in crystalline **1** and moderately fast in crystalline **2**, a fast degenerate proton tautomerism is observed for adsorbed **1** and **2**, similar to the liquid solution. Because of the different proton dynamics the line contributionns of adsorbed and bulk pyrazoles are easily distinguished. By analysis of the environment-dependent ^{1}H–^{15}N cross-polarization, efficiency quantitative information about the distribution of **2** between the bulk crystalline phase and the silica surface was obtained as a function of both types of sample preparation. The results are compatible with a monomolecular coverage of the silica surface by **2**. Whereas the state of the adsorbate is not dependent of the type of sample preparation, the surface area accessible for **2** is smaller in the case of the mechanically grinded components as compared to the case of solvent-assisted loading. This result can be modeled in terms of the fractal dimension of the silica surface and slow diffusion of the adsorbate in the latter during the time of grinding. The nature of the proton transfer of **2** adsorbed on silica was studied by low-temperature ^{15}N CPMAS NMR spectroscopy. The slow proton exchange regime is reached below 250 K. The spectral changes and their comparison with the spectra of the corresponding hydrochloride reveal that (i) **1** and **2** are adsorbed as the neutral species (ii) that there are different adsorption sites where **1** and **2** experience not only different chemical shifts but also different rate constants of proton exchange. At room temperature, site exchange, rotational diffusion, and proton exchange are faster than the Larmor frequency difference between the protonated and nonprotonated ^{15}N atoms. Since the proton exchange in the cyclic pyrazole homoassociates is much slower than in the adsorbed state, it follows that it is catalyzed by OH groups on the alumina and silica surface.

Introduction

One of the main interests of high-resolution solid-state NMR spectroscopy is the possibility of obtaining information on matrix effects on molecules and their reactivity on a time scale of slow molecular motion. Solid matrices may modulate not only molecular geometries and structures[2-4] but also the dynamics of chemical transformations. Since the latter generally require a certain molecular configuration or mobility, they are often suppressed in the solid state. Processes which have, nevertheless, been observed in crystalline solids by NMR are conformational dynamics,[5-7] fluxional behavior[8-13] and prototropy.[14-45] In some cases it has been possible to manipulate the dynamics of the prototropy by varying the solid environment from which interesting insights into the proton transfer mechanism could be obtained. For example, the intramolecular prototropy of certain dyes could be influenced by changing the crystal structure[22] or by preparing solid solutions in polystyrene.[30]

Among the solid matrices, which are important in chemistry, range porous solids such as silica and alumina, used for column or thin-layer chromatography, or zeolites, used as catalysts. The interaction of adsorbed molecules with the inner surface of these materials has been studied via IR spectroscopy[46] and different solid-state ^{13}C and ^{15}N NMR methods,[47-53] under the conditions of proton cross polarization (CP) and magic angle spinning (MAS). Thus, it has been shown that porous acidic solids offer different binding sites for ammonia, trimethylammonia, and pyridine. When pyridine and trimethylammonia are adsorbed in zeolites, pyridine becomes protonated by Brønsted sites, whereas ammonia is only protonated if more than one molecule is adsorbed per acid site.[47-55] By contrast, pyridine is not protonated by anhydrous γ-alumina where it can form various Lewis sites.[50] Under certain conditions exchange between different sites was observed.[52] So far, these studies focused on volatile adsorbates which could be adsorbed via the gas phase. Recently, Ebener et al.[56] showed by ^{13}C CPMAS NMR, that larger nonvolatile benzenoid aromatics (MW > 120) can also be incorporated into silica or alumina surfaces by mixing and mechanically grinding the components or by solvent-assisted mixing. Even the larger adsorbed molecules were found to be subject to rotational diffusion processes which almost completely average out the ^{13}C–^{1}H dipolar interactions and the ^{13}C chemical anisotropy. As a consequence, the ^{13}C NMR line widths were found to be smaller than in the case of the bulk solids and almost as good as in liquid solution.

These results incited us to mix heterocyclic compounds which are subject to a well-defined proton tautomerism in the bulk crystalline state with silica and alumina and to study the effect of mixing on the proton-exchange dynamics by high-resolution solid-state CPMAS NMR spectroscopy. Such systems are expected to serve as models for fast bond-breaking and bond-formation processes in the adsorbed state. The compounds we actually chose to study stem from the class of pyrazoles which are bifunctional proton donor/acceptors characterized by an annular proton tautomerism[45] in the bulk solid state. Depending on the substituents these molecules form either infinite hydrogen-

® Abstract published in *Advance ACS Abstracts*, July 15, 1994.

0022-3654/94/2098-8752$04.50/0

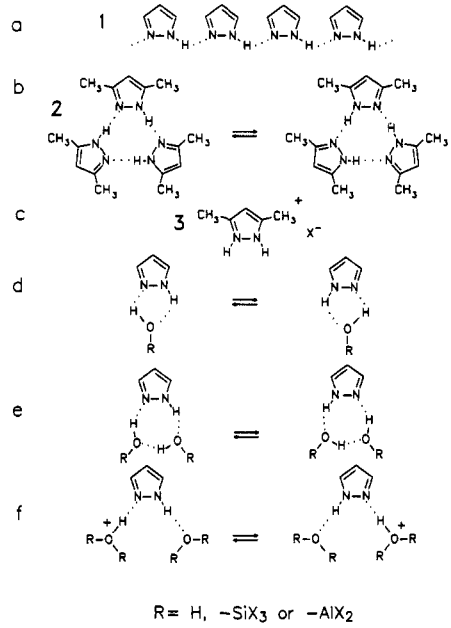

Figure 1. (a) Hydrogen-bonded structure of solid pyrazole **1** (schematically),[57] where proton exchange is suppressed.[34] (b) Cyclic trimers in crystalline dimethylpyrazole[41] in which a degenerate triple proton transfer takes place.[40-42] (c) Structure of protonated dimethylpyrazole **3**. (d and e) cyclic proton exchange of pyrazole with silica and alumina surface OH groups or water. (f) proton exchange of pyrazole linking two Brønsted sites.

bonded chains (Figure 1a) in which the tautomerism is suppressed[33-38,57] or cyclic dimers, trimers (Figure 1b), or tetramers which are subject to degenerate double, triple, or quadruple proton-transfer processes.[40-42] The latter have been studied either by ^{13}C or, after isotopic labeling, by ^{15}N CPMAS NMR spectroscopy.[34-42] To explore surface effects on the annular tautomerism of typical pyrazoles, we chose a representative of both pyrazole types, i.e., the parent compound pyrazole **1** and 3,5-dimethylpyrazole (**2**). The first forms nonexchanging hydrogen-bonded chains[34,57] and the second, exchanging cyclic trimers[40-42] in the bulk crystals.

In the following, the ^{13}C and ^{15}N CPMAS NMR experiments performed are described and discussed. It is shown that pyrazole and 3,5-dimethylpyrazole are incorporated into the silica and alumina surfaces as the neutral molecules. A comparison of the spectra obtained with those of the bulk solids reveals substantially different proton-exchange characteristics ascribed to the interaction with acidic surface OH groups. These processes may involve either protonated intermediates according to Figure 1c or coupled proton-transfer pathways as illustrated in Figure 1d–f.

Experimental Section

Compounds. Nonlabeled pyrazole (mp 68–70 °C) and 3,5-dimethylpyrazole (mp 107–109 °C) for the ^{13}C CP NMR experiments were purchased from Aldrich. Their purity was checked by solution ^1H NMR spectroscopy at 200 MHz. [$^{15}N_2$]-pyrazole and 3,5-dimethyl[$^{15}N_2$]pyrazole were prepared according to refs 57 and 41. The porous adsorbents were purchased from Merck Chemical Co. and were characterized as follows: (i) Neutral alumina Merck 90 for chromatography (γ-alumina), product no. 1077: Gaussian pore size distribution, average pore diameter 90 Å, half-width of the distribution approximately 30 Å, corn size 63–200 μm (70–230 mesh ASTM), inner pore surface 120 m^2/g, pore volume 0.35 mL/g; (ii) Silica Merck 60 for chromatography, product no. 9385: Gaussian pore size distribution, average pore diameter 60 Å, half-width of the distribution approximately 20 Å, corn size 40–63 μm (230–400 mesh ASTM), inner pore surface 500 ± 30 m^2/g, pore volume 0.7 mL/g. The outer surface of the adsorbents is negligibly small. According to the manufacturer, paramagnetic impurities are absent in these materials. When purchased, they contain approximately 5% water. Apart from silica and alumina, $CaSO_4$ powder and KBr pellets were also checked as matrices. Calcium sulfate was purchased from Aldrich, product no. 23,713-2.

Sample Preparation. In the first stage, water was partly removed from the adsorbents by drying over P_2O_5 for 1 week at 70 °C and 10^{-6} bar. Contact with air was avoided as far as possible when preparing the samples. The latter were prepared in a manner similar to the recipe of Ebener et al.[56] in two different ways: (i) by mixing and mechanically grinding the components; (ii) by solvent-assisted adsorption. In the first procedure, the dried adsorbents (silica 60 or alumina 90) and the adsorbates **1** or **2** were mixed in a mortar under an argon atmosphere and grinded with a pestle for 10 min until a homogeneous mixture was obtained. In the second procedure, the adsorbent and adsorbates were mixed and digested for 1 or 2 min with 5 mL of absolute CH_2Cl_2 using Schlenk techniques under an argon atmosphere. The solvent was then carefully removed *in vacuo*, and finally the resulting powders were loaded under argon into the NMR rotors. Dry nitrogen evaporated from liquid nitrogen was used as driving and bearing gas. Although contact with air was avoided as much as possible, we estimate the water content in the final samples to be about 1–2%. In the case of the samples prepared by solvent-assisted loading, no evidence for residual surface solvent could be obtained by solid-state ^{13}C MAS NMR. No loss of the adsorbate into the surrounding atmosphere during the grinding process could be detected within the margin of error, which is understandable because of the low volatility of **1** and **2** at room temperature. Finally, we note that the weight/weight mixing ratios were

$$R = (m_a + m_b)/m_{ads} \quad (1)$$

where m_a and m_b are the masses of adsorbed and bulk **1** and **2** in the sample, and m_{ads} is the mass of the adsorbent. R was varied between 1 and 0.125.

NMR Spectroscopy. The solid-state ^{13}C CPMAS NMR spectra were recorded on a Bruker AC 200 spectrometer working at 50.32 MHz, using a 7-mm Bruker DAB 7 probehead which achieves rotation frequencies of about 3.5–4.5 kHz. The standard CPMAS pulse sequence was applied with a 7 μs ^1H 90° pulse width, 3–5 ms contact pulses, and 5 s repetition time, the spectral width being 20 kHz. All chemical shifts are given with respect to the spectrometer reference frequency which was calibrated by the glycine signal at 176.1 ppm. The ^{15}N CPMAS NMR spectra were recorded on a Bruker MSL 300 spectrometer working at 300.13 MHz for protons and 30.41 MHz for ^{15}N. The spectrometer was equipped with a 5-mm high-speed CPMAS probehead from Doty Scientific, USA. The spinning speeds were of the order of 8–8.5 kHz. Because of sample heating associated with these high speeds,[32] the sample temperatures were, when necessary, determined by addition of a small capsule into the rotor containing between 0.5 and 2 mg of the ^{15}N chemical shift thermometer TTAA. A Bruker B VT 1000 temperature unit was used to control the temperature of the bearing nitrogen gas stream and a homemade heat exchanger to achieve low temperatures. The standard CPMAS pulse sequence was again applied here: 5 μs ^1H 90° pulse width, 4–12 ms CP time and 4 s recycle delay, spectral width of 15 000 Hz. All ^{15}N chemical shifts are related to external solid $^{15}NH_4Cl$, ppm values for narrow lines are given with an error of ±0.3 ppm, broadened lines with ±0.5 ppm.

Results

Qualitative Solid-State ^{13}C and ^{15}N CPMAS NMR Spectroscopy. During the first stage of this study, ^{13}C CPMAS NMR spectra were recorded for samples of **1** and **2** adsorbed on the

TABLE 1: Chemical Shifts in ppm of Pyrazoles[a]

	T/K[d]	C-3	C-5	C-4	CH_3-3	CH_3-5	N-1	N-2
1 CH_2Cl_2	298	134.6[59]	134.6[59]	105.8[59]				
1 DMSO	RT						177[60,61]	270[60,61]
1 $CDCl_3$	RT						216[60]	216[60]
1 crystal	RT	139[34]	128[34]	107[34]			170	248
1 Si, S4, S8	RT	134[b]	134[b]	105				
1 Al, M1, S1,	RT	134[b]	134[b]	105				
		139[c]	128[c]	107				
1 Al, S4, S8	RT	135[b]	135[b]	106				
1 $CaSO_4$	RT	139[c]	128[c]	107				
1 Al, M4	RT						170[c]	248[c]
							208[b]	208[b]
1 Al, S4	RT						207[b]	207[b]
1 Si, M4	RT						204[b]	204[b]
2 CH_2Cl_2	298	145.3[59]	145.3[59]	104.8[59]	12.9[59]	12.9[59]		
2 crystal	368	143[40]	143[40]	105[40]	12[40]	12[40]	204[41,42]	204[41,42]
2 crystal	260	146[40]	141[40]	105[40]	12[40]	12[40]	167[41,42]	241[41,42]
2 Si, M4	305						198[b]	198[b]
2 Al, M4	305						168[c]	243[c]
2 Al, M8	305						169[c]	241[c]
							200[b]	200[b]
3	305						154	154

[a] Reference: tetramethylsilane for ^{13}C, $^{15}NH_4Cl/H_2O$ or solid $^{15}NH_4Cl$ for ^{15}N. In order to obtain ^{15}N chemical shifts with CH_3NO_2 as reference a value of 353 ppm has to be substracted. DMSO, $CDCl_3$: liquid-state NMR spectra using dimethyl sulfoxide-d_6 or deuteriochloroform as solvents. Crystal: CPMAS NMR measurements performed on crystalline material. Si, Al, $CaSO_4$: CPMAS NMR experiments using silica, alumina of calcium sulfate as adsorbent. MX: samples prepared by mechanical grinding of 1 part adsorbate and X parts w:w of adsorbent, i.e., a mixing ratio of $R = 1/X$. SX: solvent (CH_2Cl_2) assisted adsorption with $R = 1/X$. [b] Line of adsorbate averaged by rapid proton transfer on the surface. [c] Microcrystals in the adsorbate/adsorbent mixture. [d] RT = room temperature.

solids mentioned in the previous section, prepared by mixing and mechanical grinding or by solvent-assisted loading. Whereas in the case of $CaSO_4$ and KBr matrices only the spectra typical for polycrystalline bulk **1** and **2** could be detected, interesting effects were found when alumina and silica were used as adsorbents. When the mixing ratio R of adsorbate and adsorbent was not too large, only one single ^{13}C signal was observed for the C-3 and C-5 positions, indicating a fast degenerate intermolecular proton tautomerism. The average chemical shifts were similar to the values obtained for solutions in $CDCl_3$ where proton exchange is also fast, as can be inferred from Table 1 in which all ^{13}C and ^{15}N NMR chemical shifts of **1** and **2** relevant in this context are assembled. Surcharging the surfaces at mixing ratios of $R >$ 0.25 led to the appearance of a superposition of subspectra typical for the adsorbed state and the bulk polycrystalline state. If n_a and n_b are the number of moles of the adsorbate on the surface and in the remaining bulk phase, the corresponding mole fractions x_a and x_b are given by

$$x_a = (1 - x_b) = n_a/(n_a + n_b) \qquad (2)$$

Because of the relatively small ^{13}C chemical shift changes associated with the tautomerism, it was somewhat difficult to extract values of x_a by ^{13}C NMR. We therefore decided to study these phenomena in more detail by ^{15}N CPMAS NMR spectroscopy, where the pyrazole nitrogen atoms experience major chemical shift changes upon protonation/deprotonation. In Figure 2 the ^{15}N CPMAS NMR spectra of **1**, **2**, and **2**·HCl ≡ **3** are depicted. The signals labeled with asterisks stem from the ^{15}N chemical shift thermometer TTAA.[32]

Let us first discuss the spectra of the bulk polycrystalline compounds. Since the tautomerism is suppressed in solid **1** due to the formation of infinite hydrogen-bonded chains[34,57] two sharp signals at 170 and 248 ppm were observed for the protonated nitrogen atom N-1 and the nonprotonated nitrogen N-2 (Figure 2a). These chemical shifts are similar to those obtained for solutions of **1** in DMSO where the proton transfer is slow, as indicated in Table 1. Differences arise from the formation of various types of hydrogen bonds in both kinds of environment and, to some extent, also from susceptibility effects associated with the particle size. The latter influence is, however, not of great consequence because of the small gyromagnetic ratio of ^{15}N; moreover, extensive mechanical grinding of bulk crystalline **1** did not lead to noticeable spectral changes. The corresponding signals of polycrystalline **2** appear at 167 and 241 ppm but are sharp only at low temperatures as shown in Figure 2d. At room temperature, the signals are substantially broadened due to a

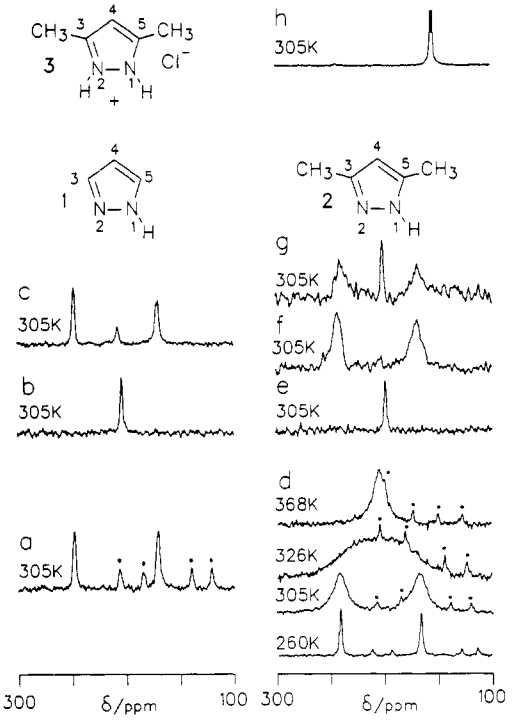

Figure 2. The 30.41-MHz ^{15}N CPMAS NMR spectra at 305 K of doubly ^{15}N-labeled pyrazole **1**, 3,5-dimethylpyrazole (**2**), and 3,5-dimethylpyrazole hydrochloride (**3**) under various conditions. All spectra were recorded at the same spinning speed of 8.2 kHz at 305 K, except the spectra in d. Asterisks: chemical shift thermometer TTAA. (a, d, h) Polycrystalline powders of **1**, **2**, and **3**. (b, e) Samples obtained by mechanical grinding of **1**, **2** with silica, mixing ratios $R = 0.25$. (c, f) Samples obtained by mechanical grinding of **1**, **2** with alumina, $R = 0.25$. (g) Sample obtained by mechanical grinding of **2** with alumina, $R = 0.125$; 8 ms CP times, 5 μs 90 ^1H pulses.

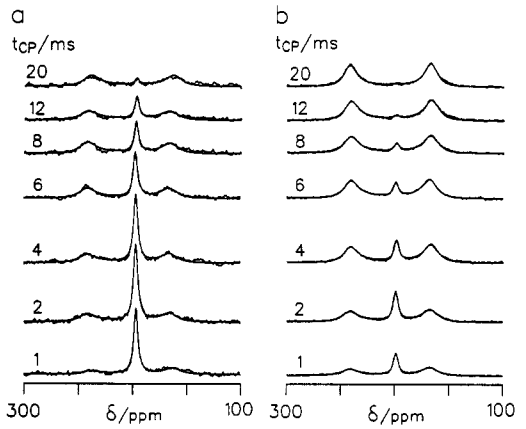

Figure 3. Room-temperature (305 K) superposed experimental and calculated 30.41-MHz ^{15}N CPMAS NMR spectra series of (a) a physical mixture (sample a) of 10 mg of bulk **2** and of 10 mg of **2** adsorbed on 40 mg of silica and (b) 30 mg of bulk **2** adsorbed on 30 mg of SiO_2 (sample b), as a function of the cross-polarization times t_{CP}. Repeating time 4 s. Parameters of the line-shape analyses were the intensities I_a^i and I_b^i of the adsorbed and bulk **2** of sample i = a, b, and the rate constants of the proton exchange, 1500 s^{-1} in bulk **2** and >50000 s^{-1} for adsorbed **2**. The vertical scaling factor was the same in each set of experiments, but different for the two samples, i.e., $F^a = 1$ and $F^b \neq 1$. For further explanation see text.

TABLE 2: Signal Intensities I_j^i of Adsorbed (i = a) and Bulk (i = b) 2 Obtained for Samples j = a and b by the Line-Shape Analysis of Figure 3

t_{CP}/ms	I_a^a	I_b^a	I_a^b	I_b^b
0.5	0.52	0.44	0.13	0.4
1	0.8	0.47	0.21	0.51
2	1.13	0.86	0.29	0.68
4	0.9	0.9	0.18	0.97
6	0.61	0.92	0.12	1.08
8	0.38	0.98	0.06	1.05
10	0.26	1.11	0.025	1.005
12	0.29	0.95	0.018	1.012
15	0.15	0.97	0.015	0.985
18	0.08	0.95	0.01	1
20	0.07	0.96	0	1.02

degenerate triple proton transfer in the cyclic trimer, as indicated in Figure 1b.[40-42] When the temperature is increased, the lines coalesce into a single line. The rate constants of the triple proton and deuteron transfer were determined by line-shape analysis.[40-42] When **2** is protonated with HCl to give polycrystalline **3**, two barely resolved lines were observed at 154 ppm, indicating a slight reduction of the molecular symmetry by the crystal field (Figure 2h). The observed high-field shift upon protonation is in agreement with the literature.[60,62] No sign of proton-transfer dynamics was observed in solid **3**.

The ^{15}N spectra of **1** and **2** obtained after mixing with silica show remarkable changes. As expected from the ^{13}C CPMAS measurements, only one single averaged ^{15}N line for N-1/N-2 at about 200 ppm is observed when neutral **1** and **2** are adsorbed by silica at mixing ratios of R = 0.25, indicating a rapid degenerate proton exchange between N-1 and N-2 (Figure 2b,e). The longitudinal relaxation time ^{15}N T_1 of the coalesced center line of **2** on silica is only 0.5 s and much smaller than the corresponding value >50 s for bulk solid **2**. An additional CP off-angle-spinning (OAS) experiment performed on this sample also yielded a sharp center line indicating a rapid isotropic motion which averages the large chemical shift anisotropy of about 370 ppm[63] of this compound. A comparison of the line positions with those of **2** at high temperature and of **3** indicates that **1** and **2** are adsorbed as the neutral species subject to a fast surface tautomerism and not as the cations. Within the margin of error, no spectral differences could be observed for samples prepared by solvent assisted adsorption or mechanical grinding (see Table 1).

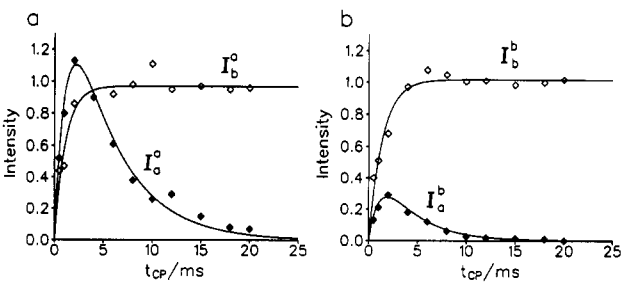

Figure 4. Plot of the intensities I_a^i and I_b^i of adsorbed and bulk **2** obtained by line-shape analysis for samples i = a and b as a function of the cross-polarization time t_{CP}. The solid lines represent the calculated values obtained by nonlinear least-squares fit in terms of eq 4.

When alumina was used as adsorbent at mixing ratios of R = 0.25 superpositions of two subspectra were observed for **1** and **2**, typical for two solid environments (Figure 2c,f): (i) the adsorbed state again characterized by a single averaged line around 200 ppm arising from fast proton exchange and (ii) the bulk crystalline material. The position of the single averaged line was slightly different compared to that of the compound adsorbed on silica (see Table 1). The fraction x_a of adsorbed **2** could be increased by adding more adsorbent at the expense of the fraction $x_b = 1 - x_a$ residing in the bulk state (Figure 2g).

Characterization of the Distribution between the Bulk Phase and the Adsorbed State by Quantitative ^{15}N CPMAS NMR Spectroscopy. The evaluation of the quantity x by ^{15}N CPMAS NMR spectroscopy is not straightforward because of the well-known problem of environment dependent ^1H–^{15}N cross-polarization dynamics leading to signal intensity distortions, i.e., the intensity I_i of signal i is related to the number of moles n_i by

$$I_i = C_i n_i \tag{3}$$

where C_i is a constant differing for each signal in the spectrum. In the case where the two different environments give rise to well resolved lines as in the cases studied here the problem can be solved as described in the following for mixtures of **2** with silica.

Firstly, we prepared a ground mixture of 10 mg of **2** with 40 mg of silica (R = 0.25) and checked that **2** was completely adsorbed. This mixture and 10 mg of bulk **2** were then placed separately in the NMR rotor. The superposed experimental and calculated room-temperature ^{15}N CPMAS NMR spectra of this sample labeled "a" are shown in Figure 3a as a function of the cross-polarization time t_{CP}. All other spectral parameters were kept constant. The repetition time was 4 s in all experiments. Parameters of each simulation were the absolute line intensity I_a^a of the center line which stems from adsorbed **2** in the mixture, and the total line intensity I_b^a of bulk **2** giving rise to the broadened outer lines of bulk **2**. The signal shape of the latter was calculated as described previously[40-42] in terms of a symmetric two-state exchange problem with a rate constant of 1500 s^{-1}. The results are assembled in Table 2. The expected intensity ratio of $I_a^a/I_b^a \approx 1$ was obtained at t_{CP} = 4 ms.

In the next experiment we measured the ^{15}N CPMAS NMR spectra of sample b, prepared by solvent-assisted loading of **2** with silica in the ratio R = 1 as a function of t_{CP} at room temperature. The results are shown in Figure 3b. The spectra are comparable to those of Figure 3a, but here bulk **2** is intimately mixed with silica. Our goal was now to measure the amount of **2** adsorbed by line-shape analysis. Assuming that the cross-polarization characteristics of adsorbed and bulk **2** are the same in sample a and in sample b, the spectrum at t_{CP} = 4 ms should give the correct signal ratio I_a^a/I_b^a. To see whether this assumption was correct in Figure 4, all intensities obtained were plotted as a function of t_{CP}. Figure 4a contains the data which stem from sample a where the same quantity of **2** is located in the bulk phase

TABLE 3: Parameters Obtained by Nonlinear Least-Squares Fit of the Data in Figure 4 in Terms of Eq 4

	adsorbed **2** (j = a) sample i = a	bulk **2** (j = b) sample i = a	adsorbed **2** (j = a) sample i = b	bulk **2** (j = b) sample i = b
$I_0(j,i)$	2.4	0.97	0.7	1.0
$T_{1\rho}(j,i)$	4.7 ms	11 s	3.4 ms	12 s
$T_{CP}(j,i)$	1.6 ms	1.1 ms	1.7 ms	1.4 ms

and the silica surface. Whereas I_b^a increases monotonously with increasing t_{CP} until a plateau is reached, I_a^a first increases to a larger value than the plateau value of bulk **2** and then decreases exponentially. This effect is caused by short T_1 and $T_{1\rho}$ values of the protons of **2** in the adsorbed state arising from a high molecular mobility, in contrast to bulk **2**. Because of the shorter T_1 values of adsorbed **2**, saturation is less pronounced and the maximum intensity greater than for bulk **2** where the T_1 values are longer. On the other hand, because of the shorter ^1H $T_{1\rho}$ values of adsorbed **2**, the cross-polarization efficiency rapidly decays at longer cross-polarization times. The different cross-polarization characteristics lead in this case to a crossing of the two curves at $t_{CP} \approx 4$ ms where the correct intensity ratio $I_a^a/I_b^a = 1$ is obtained. The data were analyzed by nonlinear least-squares fit in terms of the usual[64] cross-polarization equation:

$$I_i = I_{0i}[(1 - \exp(-t_{CP}/T_{CP}^i))\exp(-t_{CP}/T_{1\rho}^i)], \qquad i = a, b \tag{4}$$

where T_{CP} is the cross polarization time constant. The obtained parameters describing the solid curve in Figure 4a are assembled in Table 3. An analysis was made in the case of sample b as indicated in Figure 4b. A look at Table 3 indicates that the values of $T_{1\rho}$ and T_{CP} in a given environment are similar in both samples a and b, although **2** was loaded into the surface in the case of sample a by grinding and in sample b with the aid of the solvent. Thus, the assumption of reproducible cross-polarization dynamics in the adsorbed state is fulfilled within the margin of error and independent of the way of loading. To obtain the mole fraction of adsorbed **2** in sample b, we proceeded as follows: From eq 3 it follows, assuming sample-independent cross-polarization factors C_i, that

$$I_a^a = FC_a n_a^a, \qquad I_a^b = C_a n_a^b$$

$$I_b^a = FC_b n_b^a, \qquad I_b^b = C_b n_b^b \tag{5}$$

where n_i^j is the number of moles in phase i and sample j and F a signal independent factor relating the intensities in experiments a and b. From eq 5 it follows that

$$I_a^a = FI_a^b n_a^a/n_a^b = f_a I_a^b \tag{6}$$

$$I_b^a = FI_b^b n_b^a/n_b^b = f_b I_b^b \tag{7}$$

Since $n_a^a = n_b^a$ in sample a, it follows from eqs 6 and 7 that the mole fraction of adsorbed **2** in sample b is given by

$$x_a = (1 - x_b) = n_a^b/(n_a^b + n_b^b) = 1/(1 + f_a/f_b) \tag{8}$$

As illustrated in Figure 5, eqs 6 and 7 are well fulfilled within the margin of error and with the values of $f_a = 4.0$ and $f_b = 0.96$ obtained by least-squares fit, we calculate a mole fraction of $x_a = 0.19$. From the intensity values I_a^b and I_b^b at $t_{CP} = 4$ ms listed in Table 2, we obtain $x_a = 0.16$. Since the value of 0.19 is based not only on a single measurement, we feel it is more reliable. However, the difference between both numbers indicates a realistic margin of error. Nevertheless, the remaining experiments of this study were performed at $t_{CP} = 4$ ms and x_a directly calculated by line-shape analysis of the resulting spectrum.

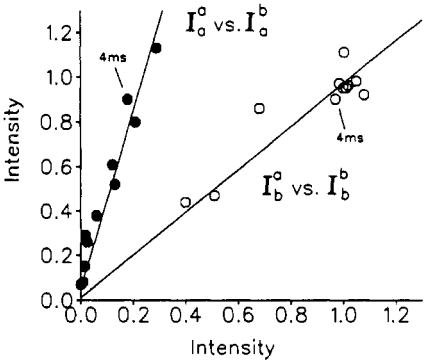

Figure 5. Data analysis of samples a and b in terms of eqs 6 and 7. For further explanation see text.

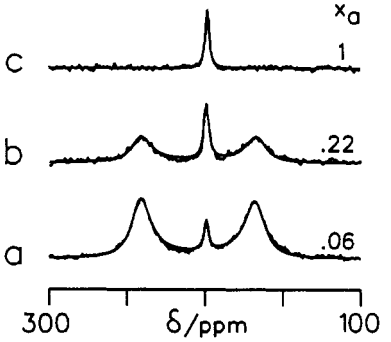

Figure 6. Room temperature (305 K) superposed experimental and calculated 30.41-MHz ^{15}N CPMAS NMR spectra of **2** under various conditions. $t_{CP} = 4$ ms, repeating time 4 s. x_a is the fraction of **2** in the adsorbed state as determined by lineshape analysis. (a) Sample c, prepared by mechanical grinding of **2** (30 mg) and of silica (30 mg), i.e., $R = 1$. (b) Sample d, where part of sample c was digested with CH_2Cl_2. (c) Sample e, obtained by grinding of 30 mg of SiO_2 and 20 mg of sample c ($R = 0.25$). The vertical scaling factor was different for each spectrum.

TABLE 4: Summary of the Samples Prepared for the Experiments Shown in Figures 3 and 6

sample	mixing ratio R with silica	way of mixing	figure
a	0.25 + bulk separate in equal amounts	grinding	3a
b	1	solvent assisted	3b
c	1	grinding	6a
d (from sample c)	1	solvent assisted	6b
e (from sample d)	0.25	grinding	6c

Our next goal was to establish whether the mode of loading, i.e., mechanical grinding and solvent-assisted loading leads to different fractions of **2** adsorbed on silica. To answer this question, we carried out the following series of experiments. We again prepared a mixture of **2** with silica with $R = 1$ by mechanical grinding (sample *c*) and found $x_a = 0.06$ through line-shape analysis of the spectrum depicted in Figure 6a. A summary of the samples prepared for the experiments shown in Figures 3 and 6 is given in Table 4. One part of sample c was then digested with CH_2Cl_2. After evaporation of the solvent *in vacuo* at 10^{-6} bar, sample d, whose spectrum is shown in Figure 6b was obtained. Via line-shape analysis, we found that the fraction of molecules adsorbed had increased to $x_a = 0.22$ which reproduces well the value of sample b. To check whether a kinetic bottleneck is responsible for the small value of x_a in sample c, 30 mg of silica was added to 20 mg of sample c and ground again resulting in sample e where $R = 0.25$. Its spectrum is shown in Figure 6c. **2** was then entirely adsorbed on the silica surface, i.e., $x_a = 1$.

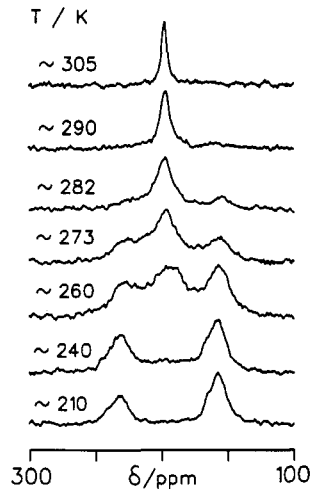

Figure 7. The 30.41-MHz ^{15}N CPMAS NMR spectra of a sample of **2** adsorbed on silica, mixing ratio $R = 0.25$, prepared by mechanical grinding as a function of temperature. For the sake of clarity the TTAA chemical shift thermometer was omitted. The sample temperatures are therefore only estimates.

Variable-Temperature ^{15}N CPMAS NMR and Tautomerism of 2 Adsorbed on Silica. To obtain further details concerning the surface proton exchange of pyrazoles adsorbed by porous solids, variable-temperature ^{15}N CPMAS experiments were performed on **2**, entirely adsorbed on silica, in a mixture ratio of $R = 0.25$. The results are shown in Figure 7. There are remarkable differences to the variable temperature ^{15}N CPMAS NMR spectra of bulk **2** depicted in Figure 2d, where the slow-proton-exchange regime was reached at 260 K characterized by two sharp lines at 167 and 241 ppm for the protonated nitrogen atoms N-1 and the nonprotonated nitrogen atoms N-2, as discussed above. In the case of **2** adsorbed on silica, the proton exchange is much faster as compared to bulk **2**, and it was necessary to lower the temperature even more in order to reach the slow-proton-exchange regime. Thus, as indicated in Figure 7, two separate lines for N-1 and N-2 appear only at 210 K at positions expected for the neutral molecules, characterized by the splitting $\Delta\nu = \nu(\text{N-2}) - \nu(\text{N-1})$ in hertz. In this temperature range the proton-exchange rates are $k \ll \Delta\nu$. There is almost no line intensity around 154 ppm where the cation **3** should absorb (see Figure 2h). Each line in the bottom spectrum of Figure 7 is much broader compared to the corresponding spectrum of Figure 2d and exhibits a barely resolved substructure. This finding indicates the presence of different environments, i.e., binding sites for **2** on the silica surface. As temperature is increased, the two lines do not simply broaden and coalesce as those of Figure 2d, but complicated spectral changes are observed which can be qualitatively understood as follows. The spectra in the temperature range between 260 and 280 K can be described in terms of a broad distribution of rate constants. This leads apparently to a superposition of two types of environments, one contributing the outer lines, characterized by small proton exchange rates, i.e., $k \ll \Delta\nu$ and the other contributing the center line where the proton exchange rates are fast, i.e., $k \gg \Delta\nu$. At 210 K only the environment with $k \ll \Delta\nu$ was observed. As temperature is increased, the environment with $k \gg \Delta\nu$ is populated. At 260 K both environments have comparable populations; at higher temperatures only the molecules with $k \gg \Delta\nu$ survive. This behavior can be explained again in terms of a distribution of different binding sites on the silica surface characterized not only by different chemical shifts but also by different rate constants k of proton exchange and, probably, also by different molecular mobilities. The center line which survives alone at room temperature is remarkably sharp, a phenomenon which is probably associated with fast exchange between the different binding sites, and, therefore, also with rapid rotational and translational jumps or diffusion of **2** on the surface, which average the anisotropy of the ^{15}N chemical shifts and the ^{1}H–^{15}N dipolar couplings. This is consistent with the above-mentioned results of the CP off-angle spinning and the T_1 measurements.

Discussion

In the previous section it was shown by ^{13}C and ^{15}N CPMAS NMR spectroscopy that the inner surfaces of alumina and silica can incorporate pyrazole **1** and dimethylpyrazole **2** (Figure 1) as the neutral species, both via mechanical grinding of the components and by solvent-assisted loading. In this state, **1** and **2** are, at room temperature, subject to a fast degenerate intermolecular proton tautomerism in contrast to the bulk crystalline environment where **1** does not exchange protons because of the formation of linear hydrogen bonded chains[34,57] and where **2** forms cyclic trimers in which the triple proton transfer is moderately fast.[40-42] The capacity of the different surfaces for pyrazole loading is finite; it depends on the type of adsorbent and adsorbate and the method of adsorption. Quantitative information concerning the distribution of **2** between the bulk crystalline state and the surface was obtained by ^{15}N CPMAS NMR. The surface proton exchange seems to be catalyzed by surface OH groups. Both cyclic multiple proton-transfer processes as well as protonation/deprotonation mechanisms (Figure 1) must be discussed. At low temperatures the surface proton exchange of **2** could be frozen out within the ^{15}N NMR time scale. In this regime, different binding sites which seem to be characterized by different proton-exchange dynamics were observed.

Let us first discuss the loading problem. The hydrophilic parts of **1** and **2** are capable of forming hydrogen bonds with proton donors and acceptors. Therefore, **1** and **2** easily form hydrogen bonds with Si–OH groups or with water in the alumina or silica surface. The free enthalpy gain of this process is apparently sufficient to compensate the enthalpy needed to break the hydrogen bonds in the molecular solids of **1** and **2** and the dissolution of the lattices. Note that we observed no signs indicating that addition of water leads to an increased incorporation of **1** and **2** into the surfaces. This leads us to believe that most of the adsorbates are directly bound to surface Si–OH groups. It will, however, be tempting in future studies to investigate whether a reduction of the latter reduces the fraction x_a of adsorbate in the surfaces.

At present, it seems that the surfaces studied contain more than one OH group per molecule of adsorbed **1** and **2**. In this regime, it is tempting to relate x_a to the size of the inner pores of the materials used. Thus, the silica used adsorbed more adsorbate than the alumina which is not surprising because the inner surface of the former was 4 times larger than of the latter. An influence of the pore diameter could not be detected. **1** is incorporated into the surfaces in larger amounts than **2** which may be ascribed to the larger molecular size of the latter. On the other hand, it is also possible that in the case of **2**, the equilibrium bulk state $\rightleftharpoons$ adsorbed state is shifted more to the bulk state, which has a higher melting point, i.e., larger intermolecular interactions in the bulk phase as compared to **1**. For the case of **2** mixed with silica in the ratio $R = 1$ it was possible to quantitatively derive values of x_a by ^{15}N CPMAS NMR spectroscopy. Let us compare the values obtained with those estimated in the following for a monomolecular coverage of the silica surface. Let n_a represent again the number of moles of adsorbed pyrazole molecules, n_b those in the bulk phase, $m_a + m_b = Rm_{ads}$ the total mass of the adsorbate, m_{ads} the mass of the adsorbent, R the mixing ratio and M the molecular mass of the adsorbate. Since $n_a = Sm_{ads}/AN_L$, where S is the inner pore surface of the adsorbent, A represents the surface covered by the adsorbate, and N_L the Avogadro's number, it follows that

$$x_a = \frac{n_a}{n_a + n_b} = \frac{n_a M}{m_a + m_b} = \frac{n_a M}{R m_{ads}} = \frac{S m_{ads} M}{R m_{ads} A N_L} = \frac{SM}{RAN_L} \quad (9)$$

A is of the order of 30–40 Å^2 when the molecular plane is perpendicular to the surface of the adsorbent as expected when **2** forms hydrogen bonds with surface OH groups as shown in Figure 1d–f, and about 50–60 Å^2 for a parallel arrangement of the molecular plane and the surface. With A = 40–60 Å^2 and S = 500 m^2/g we obtained x_a = 0.20–0.13 when R = 1. Experimentally (Figure 6), it was found for mechanically ground mixtures of **2** with silica that x_a = 0.06; however, $x_a \approx 0.16$–0.22 was found when CH_2Cl_2 was used to load **2** into the surface. The latter value is in good agreement with the values calculated from eq 9 supporting a monomolecular coverage determined by the available surface size meaning that the number of OH groups are not the bottleneck.

How can one understand that the coverage is larger after solvent-assisted adsorption as compared to mechanical grinding? It cannot be due to a different sample composition as the solvent is removed after sample preparation and as the mobility and reactivity of the adsorbate is identical in both samples. Our results can, however, be explained in terms of the model shown in Figure 8. Let us assume that during mechanical grinding (Figure 8a) the silica surface and the surface of the adsorbate microcrystals must come into contact for the mass transport from the microcrystal into the porous solid to occur. The activation energy required for the mass transport across the phase boundaries is provided by friction and stops immediately after grinding is finished. This transport is probably assisted by melting of the adsorbate surface during friction. The inner surface of the mesopores is now of fractal dimensions[66] as illustrated in Figure 8. Thus, in the solvent-assisted way of mixing, the surface accessible for the solution is relatively large because of the small size of the molecules involved. However, the microcrystals are much larger and the effective adsorbent surface experienced by these particles is, therefore, smaller. Therefore, there are remote surface areas which are not accessible by the microcrystals as illustrated in Figure 8b. Surface regions exposed to the microcrystals are now rapidly loaded and saturated during the grinding process. To load the total surface by grinding, surface diffusion of the adsorbent into remote areas is required which is slow in comparison to the grinding time despite a high local molecular mobility. If, at this point, fresh adsorbent is added to a ground mixture containing a substantial amount of microcrystals, further grinding results in their dissolution. As long as there is sufficient free surface contacting the microcrystals, no kinetic bottleneck for the adsorption process can occur; the bottleneck arises only after this surface is loaded. By contrast, there is no major bottleneck in solvent-assisted adsorption because the liquid can penetrate remote areas.

Let us now discuss in more detail the information on the reactivity and mobility of the adsorbents in the surface arising from the variable-temperature ^{15}N CPMAS NMR spectra of **2** on silica shown in Figure 7. No evidence for the formation of the cation **3** was obtained in the temperature range covered. Slightly different chemical shifts of **2** in alumina, silica, bulk crystal, and DMSO solution (Table 1) can be explained by the formation of different types of hydrogen bonds. Hydrogen-bond effects on pyrazole chemical shifts have, for example, been noticed recently.[38] In the case of **2** adsorbed on alumina and silica, small amounts of paramagnetic impurities in the latter could lead to more or less strong shifts of the ^{15}N resonances. The formation of different hydrogen bonded environments can also explain the finding of a very broad distribution of different sites characterized by different rate constants of proton exchange in **2** adsorbed on silica. A distribution of equilibrium constants of proton exchange must possibly be taken into account. Similar spectral features

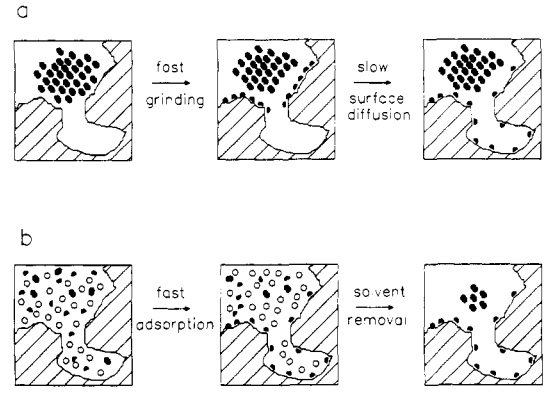

Figure 8. Model of adsorption (a) by mixing and mechanically grinding the components without solvent and (b) by solvent assisted adsorption. For further explanation see text.

have also been found for other dynamic processes in disordered matrices.[26,66,67] Distributions of this kind lead to a very small fraction of molecules exhibiting a line shape at the coalescence point, i.e., to a superposition of subspectra characteristic for the sites with slow and fast molecular dynamics. Other sources which may complicate the interpretation of the spectra are (i) a broad distribution of equilibrium constants,[30] (ii) line broadening arising from the molecular dynamics, i.e. proton exchange within the sites, and (iii) exchange between different sites. To obtain quantitative information, a detailed line-shape analysis and two-dimensional NMR experiments would be necessary, but such experiments were beyond the scope of this study.

Returning to Figure 7, at 273 K, different sites characterized by slow and by rapid proton-exchange rates give rise to broadened but distinct lines. This indicates that site-exchange processes are much slower than the proton-exchange processes; in other words, the observed proton-transfer processes take place in local hydrogen-bonded associates. Site exchange is now connected with both molecular rotational and translational jumps and diffusion processes in the surface. At the molecular level, these processes are fast at room temperature, which explains the short T_1 and $T_{1\rho}$ values in the adsorbed state as well as the observation of a sharp line in the off-angle spinning spectrum of adsorbed **2**. These observations indicate motional averaging of the anisotropy of the ^{15}N chemical shifts and of the ^{1}H–^{15}N dipolar couplings. Only the proton exchange leads to an averaging of the two ^{15}N isotropic chemical shifts of the pyrazoles studied.

What is then the mechanism of proton transfer on the surface? By comparison of the spectra obtained for **2** on silica with those obtained for bulk **2** and for other pyrazoles,[40–42] it is obvious that the proton exchange of pyrazoles loaded into alumina and silica surfaces is significantly faster than all proton-transfer processes in cyclic hydrogen-bonded dimers, trimers, or tetramers of pyrazoles in the bulk solid state. Therefore, it is unlikely to assume that the pyrazoles embedded in porous solids are subject to proton self-exchange processes. A more plausible explanation would be that the proton exchange takes place between pyrazole molecules and surface OH groups, the latter acting in different ways. The first possibility open to discussion concerns the formation of a small fraction of pyrazole cations **3** (Figure 1c). However, no evidence for the formation of such cations was obtained in this study. This is understandable, in view of the small pK_a value of 2.48 for the diprotonated cation of pyrazole.[68] The corresponding values are 9.25 for ammonium[69] and 5.17 for pyridinium,[70] explaining why ammonia and pyridine are protonated by acidic OH groups of alumina, silica and zeolites.[48–55] Nevertheless, although protonated pyrazole cations could not be directly observed, they may represent intermediates of the proton exchange between pyrazoles and acidic surface OH groups.

Other possible proton-transfer pathways are listed in Figure 1d–f which involve multiple proton transfers in cyclic hydrogen-

bonded complexes of pyrazoles with surface OH groups. It is evident that different processes could take place in various molecular sites.

Conclusions

It has been shown by high-resolution ^{13}C and ^{15}N solid-state NMR spectroscopy under the conditions of cross polarization (CP) and magic angle spinning (MAS) that alumina and silica surfaces can incorporate bifunctional proton donor/acceptor systems such as pyrazoles. The incorporation was achieved as proposed by Ebener et al.[56] both by solvent assisted loading and by mechanical grinding. By adjusting the conditions of ^{15}N CPMAS NMR, it was possible to measure the ratio of the incorporated adsorbates versus the bulk crystalline environment in a quantitative way, depending on the nature of the adsorbents, the nature of the pyrazole adsorbates and the method of loading. A model was proposed for the two loading processes. Whereas in the former the solution of the adsorbate in the organic solvent has access to a large inner surface, only a smaller portion is accessible for mass transport by grinding. Once these areas are loaded the adsorbate must first reach the remote surface areas by diffusion before more adsorbate can be loaded again by grinding.

The surfaces of silica and alumina offer different pyrazole binding sites characterized by slightly different chemical shifts. Acidic surface OH groups do not protonate pyrazole to an observable extent but rapidly exchange protons with the latter. A large distribution of binding sites characterized by different rate constants of proton transfer is present; site exchange is slow and not required for the proton transfer to occur.

In conclusion, pyrazoles constitute useful molecular probes for exploring the structure of porous solids. In addition, when using these materials as matrix for high-resolution solid-state NMR spectroscopy, one must bear in mind that proton-exchange processes can occur if the adsorbates contain mobile protons. In the future, it would be tempting to study the effects of the number of available surface water and Si–OH groups on the efficiency of the adsorption process, as well as kinetic hydrogen/deuterium isotope effects on the proton exchange of adsorbed pyrazoles and related compounds.

Acknowledgment. We thank the European Community for financial support [Project SCI 0045.C(H)]. C.L. acknowledges a grant from the "Consejería de Educación y Cultura de la Comunidad de Madrid" in order to do several experiments in Berlin; H.H.L. expresses thanks to the Fonds der Chemischen Ind. for financial support.

References and Notes

(1) (a) Freie Universität Berlin, D-14195 Berlin, F.R.G. (b) Facultad de Ciencias, UNED, E-28040 Madrid, Spain. (c) Instituto de Química Médica, C. S. I. C., E-28006 Madrid, Spain.
(2) Fletton, R. A.; Lancaster, R. W.; Harris, R. K.; Kenwright, A. M.; Packer, K. J.; Waters, D. N.; Yeadon, A. *J. Chem. Soc., Perkin Trans. 2* **1986**, 1705.
(3) Doherty, C.; York, P. *Int. J. Pharm.* **1988**, *47*, 141.
(4) Ripmeester, J. A. *Chem. Phys. Lett.* **1986**, *74*, 2721.
(5) Möller, M.; Gronski, W.; Cantow, H. J.; Höcker, H. *J. Am. Chem. Soc.* **1984**, *106*, 5093.
(6) Masek, B. B.; Santarsiero, B. D.; Dougherty, D. A. *J. Am. Chem. Soc.* **1987**, *109*, 4373.
(7) Etter, M. C.; Hoye, R. C.; Vojta, G. M. *Cryst. Rev.* **1988**, *1*, 281.
(8) Miller, R. D.; Yannoni, C. S. *J. Am. Chem. Soc.* **1980**, *102*, 7396.
(9) Meier, B. H.; Earl, W. L. *J. Am. Chem. Soc.* **1985**, *107*, 5553.
(10) Yannoni, C. S.; Johnson, R. D.; Meijer, G.; Bethune, D. S.; Salem, J. R. *J. Phys. Chem.* **1991**, *95*, 9.
(11) Tycko, R.; Haddon, R. C.; Dabbagh, G.; Glarum, S. H.; Douglass, D. C.; Mujsce, A. M. *J. Phys. Chem.* **1991**, *95*, 518.
(12) Benn, R.; Grondrey, H.; Nolte, R.; Erker, G. *Organometallics* **1988**, *7*, 777.
(13) Heyes, S. J.; Green, M. L. H.; Dobson, C. M. *Inorg. Chem.* **1991**, *30*, 1930.
(14) Harris, R. K.; Jonsen, P.; Packer, K. J.; Campbell, D. D. *J. Chem. Soc., Perkin 2* **1987**, 1383.
(15) Etter, M. C.; Urbanczyk-Lipkpwska, Z.; Jahn, D. A.; Frye, J. S. *J. Am. Chem. Soc.* **1986**, *108*, 5871.
(16) Imashiro, F.; Maeda, S.; Takeogoshi, K.; Terao, T.; Saika, A. *J. Am. Chem. Soc.* **1987**, *109*, 5213.
(17) Szeverenyi, N. M.; Bax, A.; Maciel, G. E. *J. Am. Chem. Soc.* **1983**, *105*, 2579.
(18) Okazaki, M.; McDowell, C. A. *J. Am. Chem. Soc.* **1984**, *106*, 3185.
(19) Limbach, H. H.; Hennig, J.; Kendrick, R. D.; Yannoni, C. S. *J. Am. Chem. Soc.* **1984**, *106*, 4059.
(20) Wehrle, B.; Limbach, H. H.; Köcher, M.; Ermer, O.; Vogel, E. *Angew. Chem.* **1987**, *99*, 914; *Angew. Chem., Engl. Int. Ed.* **1987**, *26*, 934.
(21) Limbach, H. H.; Wehrle, B.; Schlabach, M.; Kendrick, R. D.; Yannoni, C. S. *J. Magn. Reson.* **1988**, *77*, 84.
(22) Schlabach, M.; Rumpel, H.; Braun, J.; Scherer, G.; Limbach, H. H. *Ber. Bunsen-Ges. Phys. Chem.* **1992**, *96*, 821.
(23) Frydman, L.; Olivieri, A. C.; Diaz, L. E.; Frydman, B.; Morin, F. G.; Mayne, C. L.; Grant, D. M.; Adler, A. D. *J. Am. Chem. Soc.* **1988**, *110*, 336.
(24) Frydman, L.; Olivieri, A. C.; Diaz, L. E.; Frydmann, B.; Kustanovich, I.; Vega, S. *J. Am. Chem. Soc.* **1989**, *111*, 7001.
(25) Limbach, H. H.; Gerritzen, D.; Rumpel, H.; Wehrle, B.; Otting, G.; Zimmermann, H.; Kendrick, R. D.; Yannoni, C. S. In *Photoreaktive Festkörper*; Sixl, H., Friedrich, J., Bräuchle, C. M., Eds.; Wahl Verlag: Karlsruhe, 1985; pp 19–43.
(26) Wehrle, B.; Limbach, H. H. *Chem. Phys.* **1989**, *136*, 223.
(27) Meier, B. H.; Storm, C. B.; Earl, W. L. *J. Am. Chem. Soc.* **1986**, *108*, 6072.
(28) Rumpel, H.; Limbach, H. H. *J. Am. Chem. Soc.* **1989**, *111*, 5429.
(29) Limbach, H. H.; Wehrle, B.; Zimmermann, H.; Kendrick, R. D.; Yannoni, C. S. *J. Am. Chem. Soc.* **1987**, *109*, 929.
(30) Limbach, H. H.; Wehrle, B.; Zimmermann, H.; Kendrick, R. D.; Yannoni, C. S. *Angew. Chem.* **1987**, *99*, 241; *Angew. Chem., Int. Ed. Engl.* **1987**, *26*, 247.
(31) Wehrle, B.; Zimmermann, H.; Limbach, H. H. *J. Am. Chem. Soc.* **1988**, *110*, 7014.
(32) Wehrle, B.; Aguilar-Parrilla, F.; Limbach, H. H. *J. Magn. Reson.* **1990**, *87*, 584. (b) Aguilar-Parrilla, F.; Wehrle, B.; Bräunling, H.; Limbach, H. H. *J. Magn. Reson.* **1990**, *87*, 592.
(33) Kol'tsov, A. I.; Elkin, A. A.; Zheglova, D. Kh. *J. Mol. Struct.* **1990**, *221*, 309.
(34) Elguero, J.; Fruchier, A.; Pellegrin, V. *J. Chem. Soc., Chem. Commun.* **1981**, 1207.
(35) Faure, R.; Vincent, E. J.; Elguero, J. *Heterocycles* **1983**, *20*, 1713.
(36) Faure, R.; Vincent, E. J.; Rousseau, A.; CLaramunt, R. M.; Elguero, J. *Can. J. Chem.* **1988**, *66*, 1141.
(37) Llamas-Saiz, A. L.; Foces-Foces, C.; Elguero, J.; Meutermans, W. *Acta Crystallogr. Sect. C* **1992**, *48*, 714.
(38) Aguilar-Parrilla, F.; Cativiela, C.; Diaz de Villegas, M. D., Elguero, J., Foces-Foces, C.; Laureiro, J. I. G.; Cano, F. H.; Limbach, H. H.; Smith, J. A. S.; Toiron, C. *J. Chem. Soc. Perkin 2* **1992**, 1737.
(39) Faure, R.; Vincent, E. J.; Rousseau, A.; Elguero, J. *Heterocycles* **1987**, *26*, 333.
(40) Baldy, A.; Elguero, J.; Faure, R.; Pierrot, M.; Vincent, E. J. *J. Am. Chem. Soc.* **1985**, *107*, 5290.
(41) Smith, J. A. S.; Wehrle, B.; Aguilar-Parrilla, F.; Limbach, H. H.; Foces-Foces, M.; Cano, F. H.; Elguero, J.; Baldy, A.; Pierrot, M.; Khurshid, M. M. T.; Larcombe-McDouall, J. B. *J. Am. Chem. Soc.* **1989**, *111*, 7304.
(42) Aguilar-Parrilla, F.; Scherer, G.; Limbach, H. H.; Foces-Foces, C.; Cano, F. H.; Smith, J. A. S.; Toiron, C.; Elguero, J. *J. Am. Chem. Soc.* **1992**, *114*, 9657.
(43) Meier, B. H.; Graf, F.; Ernst, R. R. *J. Chem. Phys.* **1982**, *76*, 767; Meier, B. H.; Stöckli, A.; Ernst, R. R. *J. Chem. Phys.* **1990**, *93*, 1502. Meyer, R.; Ernst, R. R. *J. Chem. Phys.* **1990**, *93*, 5518.
(44) Heuer, A.; Haeberlen, U. *J. Chem. Phys.* **1991**, *95*, 4201.
(45) Nagaoka, S.; Terao, F.; Imaschiro, F.; Saika, A.; Hirote, N. *J. Chem. Phys.* **1983**, *79*, 4694.
(46) Elguero, J.; Marzin, C.; Katrizky, A. R.; Linda, P. *The Tautomerism of Heterocycles*; Academic Press: New York, 1976; p 313.
(47) Parry, E. P. *J. Catal.* **1963**, *2*, 371.
(48) Michel, D.; Germanus, A.; Pfeifer, H. *J. Chem. Soc., Faraday Trans. 1* **1982**, *78*, 237.
(49) Pfeifer, H.; Meiler, W.; Deininger, D. *Annu. Rep. NMR Spectrosc.* **1983**, *15*, 291.
(50) Ripmeester, J. A. *J. Am. Chem. Soc.* **1983**, *105*, 2925.
(51) Majors, P. D.; Ellis, P. D. *J. Am. Chem. Soc.* **1987**, *109*, 1648.
(52) Maciel, G. E.; Haw, J. F.; Chuang, S.; Hawkins, B. L.; Early, T. A.; McKay, D. R.; Petrakis, L. *J. Am. Chem. Soc.* **1983**, *105*, 5529.
(53) Earl, W. L.; Fritz, P. O.; Gibson, A. A. V.; Lunsford, J. H. *J. Phys. Chem.* **1987**, *91*, 2091.
(54) Vega, A.; Luz, Z. *J. Phys. Chem.* **1983**, *91*, 365. Luz, Z.; Vega, A. *J. Phys. Chem.* **1987**, *91*, 374.
(55) Teunissen, E. H.; van Santen, R. A.; Jansen, A. P. J.; van Duijneveldt, F. B. *J. Phys. Chem.* **1993**, *97*, 203.
(56) Ebener, M.; von Fircks, G.; Günther, H. *Helv. Chim. Acta* **1991**, *74*, 1296.
(57) Berthou, J.; Elguero, J.; Rérat, C. *Acta Crystallogr.* **1970**, *26B*, 1880.
(58) Fruchier, A.; Pellegrin, V.; Claramunt, R. M.; Elguero, J. *Org. Magn. Reson.* **1984**, *22*, 473.
(59) Begtrup, M.; Boyer, G.; Cabildo, P.; Cativiela, C.; Claramunt, R. M.; Elguero, J.; García, J. I.; Toiron, C.; Vedsø, P. *Magn. Reson. Chem.* **1993**, *31*, 107.

(60) Witanowski, M.; Stefaniak, L.; Szymanski, S.; Januszewski, H. *J. Magn. Reson.* **1977**, *28*, 217.
(61) Chen, B. C.; von Philipsborn, W.; Nagarajan, K. *Helv. Chim. Acta* **1983**, *66*, 1537.
(62) Schuster, I. I.; Dyllick-Brentzinger, C.; Roberts, J. D. *J. Org. Chem.* **1979**, *44*, 1765.
(63) Hoelger, Ch. Ph.D. Thesis, Berlin **1994**.
(64) Mehring, M. High Resolution NMR in Solids. *NMR Basic Principles and Progress*, 2nd ed.; Springer: Berlin, 1978; Vol. 11.
(65) Myrrhe, P. C.; Krüger, J. D.; Hammond, B. L.; Lok, S. M.; Yannoni, C. S.; Macho, V.; Limbach, H. H.; Vieth, H. M. *J. Am. Chem. Soc.* **1984**, *106*, 6079.
(66) Pfeifer, P. *Chimia*, **1985**, *39*, 120.
(67) Schulz, M.; v. d. Est, A.; Rössler, E.; Kossmehl, G.; Vieth, H. M. *Macromolecules* **1991**, *24*, 5040.
(68) Catalán, J.; Abboud, J. L. M.; Elguero, J. *Adv. Heterocycl. Chem.* **1987**, *41*, 250.
(69) Bell, R. P. *The Proton in Chemistry*; Chapman and Hall: London, 1959; Chapter 6.
(70) McDaniel, D. H.; Brown, H. C. *J. Am. Chem. Soc.* **1955**, *77*, 3756.